Journal of
Composites Science

MDPI

Article

Surface Damage in Woven Carbon Composite Panels under Orthogonal and Inclined High-Velocity Impacts

Veronica Marchante Rodriguez [1], Marzio Grasso [1,*], Yifan Zhao [1], Haochen Liu [1], Kailun Deng [1], Andrew Roberts [2] and Gareth James Appleby-Thomas [2]

[1] School of Aerospace, Transport and Manufacturing, Cranfield University, Cranfield MK43 0AL, UK
[2] Centre for Defence Engineering, Cranfield University, Defence Academy of the United Kingdom, Shrivenham SN6 8LA, UK
* Correspondence: marzio.grasso@cranfield.ac.uk

Abstract: The present research is aimed at the study of the failure analysis of composite panels impacted orthogonally at a high velocity and with an angle. Woven carbon-fibre panels with and without external Kevlar layers were impacted at different energy levels between 1.2 and 39.9 J. Sharp and smooth gravels with a mass from 3.1 to 6.7 g were used to investigate the effects of the mass and the contact area on the damage. Optical microscopy and thermography analyses were carried out to identify internal and surface damage. It was identified that sharp impactors created more damage on the impacted face of the panels, while the presence of a Kevlar layer increased the penetration limit and reduced the damage level in the panel at a higher energy.

Keywords: impact tests; gas gun; damage analysis; optical microscopy; thermography

Citation: Rodriguez, V.M.; Grasso, M.; Zhao, Y.; Liu, H.; Deng, K.; Roberts, A.; Appleby-Thomas, G.J. Surface Damage in Woven Carbon Composite Panels under Orthogonal and Inclined High-Velocity Impacts. *J. Compos. Sci.* **2022**, *6*, 282. https://doi.org/10.3390/jcs6100282

Academic Editors: Jiadeng Zhu and Francesco Tornabene

Received: 1 August 2022
Accepted: 16 September 2022
Published: 26 September 2022

1. Introduction

Composite materials are widely used in automotives and motorsports, as their design flexibility and mechanical properties enable the advanced light weighting needed to achieve high competitiveness. However, composites do not tolerate impact damage due to their limited ductility and significant sensitivity to the strain rate. Small flying objects can damage the aerodynamic surfaces of racing cars, thus greatly influencing their performance and the safety of the driver. The FIA regulates the size and shape of the gravel on every circuit, resulting, in most cases, in either spherical or river-washed stones (from 5 to 15 mm in diameter).

Four different types of impact can be defined depending on the velocity achieved by the impactor [1], namely: low-velocity impacts (LVIs) below 11 m/s, high-velocity impacts (HVIs) below 500 m/s, ballistic impacts below 2000 m/s, and hypervelocity impacts above 2000 m/s. The main difference in the structural response among these types of impacts is the deformation induced, since the higher the velocity is, the more localized the effect will be, with a high shear compared to bending for low-velocity impacts. LVIs are dominated by the global response of the panel, and HVIs are dominated by the local response (Figure 1) [2,3].

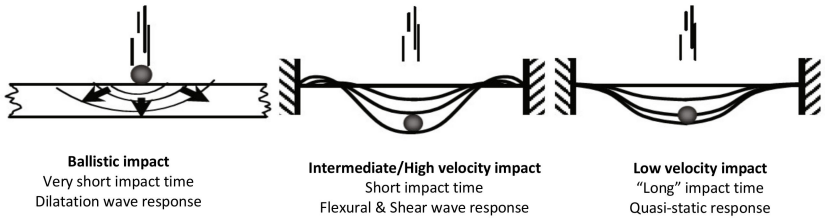

Figure 1. Comparison of high- and low-velocity impact responses (adapted from [4]).

The limit between low- and high-velocity impacts is very difficult to identify, as it will depend on the shape and geometry of the impactor, the target characteristics, and external factors, such as temperature [5]. However, in a low-velocity impact, the duration of the contact time allows elastic waves to propagate through a large portion of the target, resulting in a global response dominated by elastic strain energy that is mainly stored in the yarns [6]. These are also responsible for the propagation of elastic waves through impacted composite panels. The damage sequence is a combination of matrix cracking and fibre fracture with delamination that involves several layers depending on the energy level and the stiffness of the panel. Failure modes and energy absorption are also greatly affected by the target's size and boundary conditions [7].

Under a high-velocity impact, most of the available energy is dissipated over a small volume close to the impact point. Stress waves propagate through the thickness of the target within a short time, causing localized damages [8]. The damage sequence is characterized by transverse shear cracks that occur at an angle of approximately 45° and close to the impact area, as well as cracks due to bending that occur on the back layer [3]. With the increase in the plate thickness, the impact velocity, and the bluntness of the projectile, shear plugging becomes a likely failure mode of the final perforation of a plate. A hole is then created, and friction will be responsible for the dissipation of part of the energy while the projectile penetrates the plate [9,10] (Figure 1).

The factors affecting the size and morphology of the damage under low- and high-velocity impacts are tensile strength, strain at failure, and density, as these are related to the wave speed and the propagation of energy [11]. Woven fabrics provide better interlaminar fracture toughness than that of unidirectional ones, resulting in less damage, as the delamination is reduced. However, the in-plane properties of woven composites are affected by the fibre architecture, and 3D composites have thorough thickness reinforcement, which allows to them provide excellent in-plane and transverse properties.

The effect of the resin on the type and shape of damage depends on the toughness and strength of the resin. Thermoplastic resins possess a greater toughness and strain to failure than thermoset. Béland [12] studied the performance of thermoplastics and thermoset resins, focussing on their toughness, indentation due to fibre breakage, and matrix plasticisation, which improved the Mode-I fracture toughness and, thus, crack propagation. Thermoplastics provide a better stress distribution along the fibres, improving fibre bonding. Vieille et al. [13] compared polyether ether ketone (PEEK) and polyphenylene sulphide (PPS) with epoxy resins to study the effect of the matrix on the delamination of woven carbon-fibre laminates under impacts and observed that the two thermoplastic resins improved the delamination resistance thanks to the fibre bridging.

Lopes et al. [14] observed that limiting the orientation angle between two consecutive plies greatly improved damage tolerance. York [15] studied different lay-up configurations and observed that anti-symmetric laminates provided the best damage tolerance, and symmetric ones provide the worst behaviour. Dorey [16] reported that composites with $+/-45^{\circ}$ surface layers provided higher impact resistance and compressive residual strength with respect to those with 0° surface plies. This was attributed to the higher flexibility of the composite, which improved its ability to absorb elastic energy [8].

Park and Jang [17] studied the influence of the stacking sequence on the low-velocity impact response of hybrid aramid–glass laminates. They reported that the placement of aramid plies at the outer surface of a carbon-fibre laminate increased the impact resistance because the fibres with a high strain to failure on the outer side could undergo greater deformation [8].

The thickness of the target and its in-plane dimensions dictate the bending stiffness, the magnitude of the maximum contact force, and the induced damages. Flexible targets are mainly influenced by bending, which causes tensile stress in the ply that is exposed to the impact, and matrix cracks and, thus, delamination are developed. This leads to the reverse-pine-tree damage. For stiffer targets, the high-stress region is located directly where the impact takes place (the pine tree) [18]. According to Gellert [19], the energy absorption

in thin-glass-fibre-reinforced targets is largely independent of the geometry of the projectile nose, and thicker composites are more ballistically efficient, as they improve indentation, which is a significant mechanism of energy absorption. At a small span-to-thickness ratio and low velocity, a high stiffness, a large peak force, and a short duration occur; thus, delamination is more likely to occur. At a high velocity, the short contact duration of the event reduces the effect of the span-to-thickness ratio [12].

Icten et al. [20] found that decreasing the diameter of the impactor results in a decrease in the impact resistance at the same energy. The most common shapes are spherical, cylindrical, flat, and diamond-shaped. Sevkat et al. [21] found that the contact duration and peak force are modified by the shape of the impactor, with a large contact area creating the highest force.

Blunt projectiles cause failure through shear plugging, while conical projectiles cause petalling in thin plates. Ductile hole enlargement is observed in thick plates, and hemispherical projectiles cause tensile stretching after a huge indentation of the target plate. During high velocity impacts, ballistic limit of blunt projectile is lower than hemispherical and conical ones [22]. Conical projectiles induce a greater local and global energy [9]. Mitrevski et al. [5] concluded that blunt hemispherical impactors produce more damages than conical and ogival ones in low-velocity impacts, whilst Lee et al. [23] reported that flat and hemispherical impactors produce similar responses.

The mass of the projectile will influence the energy absorption mechanisms of the target. Small masses cause limited damage at low velocity and greater localised damages at high velocity because an increase in mass will induce a shift from global to local in the failure mechanisms. Small masses cause through-thickness waves, intermediate masses involve shear and flexural waves, and large masses involve a quasi-static response [1].

Fibre hybridisation has been reported to improve impact response when used in combination with a given lay-up. Hazell et al. [24] performed high-velocity tests and compared the effects of adding Kevlar layers in different places. When penetration occurred, placing the layer on the face that was directly impacted was the least effective solution. Gustin et al. [25] used Kevlar for low-velocity impacts and observed a 10% increase in absorbed energy.

The current literature reviewed for this work deals with the ballistic limit and internal damages produced during high-velocity impacts. There is very little related to the impact response of composite panels under inclined im-pact with incident angle close to 0° or 180° degree. The experimental data were collected at energy levels below those corresponding to the ballistic limit of the composite panel. This characterization is aimed at the definition of damage mechanisms in order to be able to devise systems (including coatings) that can be used to protect surfaces and reduce damages.

Thus, in this work, hybrid composite plates made with woven carbon and Kevlar fabrics were tested with a gas gun that used gravel with smooth and sharp surfaces at different incident angles. Then, the damaged surfaces were analysed with optical microscopy and thermal imaging to correlate the surface damages, energy levels, and gravel shapes.

2. Materials and Methods

In order to study the effects of high-velocity impacts on carbon-fibre-reinforced polymers (CFRPs) and a hybrid configuration with an external layer of Kevlar, the first step was to perform experimental tests with a wide range of impact velocities at two different impact angles of 0°and 88°. The composite laminates used in this study were manufactured at Cranfield University using pre-impregnated 5HS CFRP supplied by Cytec, which consisted of 5HS woven carbon 3K Toray T1000 fibres and MTM49 toughened epoxy [24] with a resin weight of 42%. The 5HS CFRP material had an areal density of 283 g/m^2, a nominal ply cure thickness of 0.35 mm, and the mechanical properties listed in Table 1. The curing cycle (pressure and temperature) followed the datasheet [24].

Table 1. Mechanical properties of MTM49-3-42%-3KFT300B40B-5H-283-1000.

Mechanical Properties	Results
0° Tensile strength (MPa)	1065
0° Tensile modulus (GPa)	44.6
90° Tensile strength (MPa)	1035
90° Tensile modulus (GPa)	42.8
0° Compressive strength (MPa)	640
0° Compressive modulus (GPa)	59
90° Compressive strength (MPa)	610
90° Compressive modulus (GPa)	57
In-plane shear strength (MPa)	108
In-plane shear modulus (GPa)	2.5
0° Interlaminar shear strength (MPa)	64.2

Ten samples were made from carbon fibre (CF) with three layers that were 0.35 mm thick each, and the other four samples were made with carbon fibre with three layers that were 0.35 mm thick each plus one layer of Kevlar that was 0.35 mm thick. All specimens were cured for 90 min at 135 °C in an autoclave oven. The test samples were cut into plates with dimensions of 150 × 100 mm with different thicknesses. Table 2 summarises details of the panels and lay-ups.

Table 2. Panel lay-up configuration.

Specimen Number	Panel Thickness (mm)	Number of Layers	Type of Fibre
1, 2, 3, 4 13, 14, 15, 16,17, 18	1.05	3	CF
5, 6, 7, 8 9, 10, 11, 12	1.40	4	CF + kevlar

2.1. Impact Testing

The impact testing was conducted using a single-stage light gas gun (Figure 2), which used compressed air to propel the projectiles. The gas gun consisted of a 1.75-m-long smooth-bore barrel with a calibre of 22 mm. Gravel was used as a projectile; this was saboted to enable the firing of sub-calibre sizes and loaded into the gun at the breech end. The breech was then sealed and the was gun charged with the correct pressure to produce the velocity required. The velocity was measured via a set of infrared LEDs and receivers, and the time between them was recorded on an oscilloscope. The gun was fired remotely via an electronic solenoid. A Phantom V1212 high-speed camera operating at 10,000 frames per second was used to record the impact and assess the residual velocity.

The composite panels were held in an aluminium-frame-type fixture, as shown in Figure 3. This fixture had a 130 × 80 mm rectangular opening. The two frames were held together using eight hex-head cap-screw alloy steel bolts to restrain out-of-plane motion and rotation. These held the panel in place without any gaps. All impacts were targeted toward the centre of the frame.

Two types of projectiles were used—projectiles with smooth and sharp surfaces—with different masses. Before the test, each projectile was weighed, and the major and minor dimensions were measured. The gravel was fired with the help of a sabot made of Styrofoam LB-X with a density of 33 kg/m^3. A summary of all of the tests conducted, including the panels, gravel weights, types, impact speeds, and energies, is presented in Table 3.

Figure 2. Picture of the setup for the gas gun and chamber.

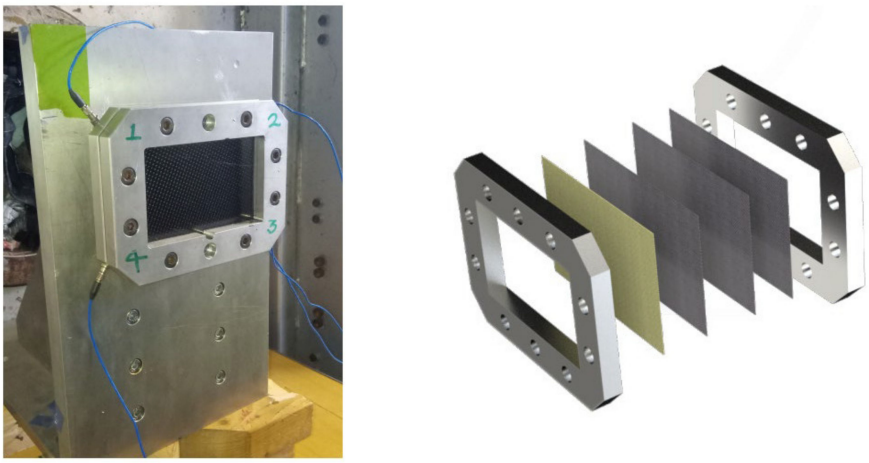

(**a**) (**b**)

Figure 3. (**a**) Image of the holding of the sample for gas gun testing and (**b**) representation of the frame and panel layers.

Table 3. Summary of the impact tests conducted and their details ("p": full penetration of the panel).

Sample Number	Panel Materials	Projectile Type	Angle of Impact	Projectile Weight (g)	Impact Velocity (m/s)	Energy (J)
1	CF	Sharp	28.5°	5.12	38.4	3.1
2 (p)	CF	Sharp	28.5°	6.12	76.9	15.4
3	CF	Smooth	28.5°	5.32	35.0	2.7
4 (p)	CF	Smooth	28.5°	5.82	68.9	11.6
5	CF + Kevlar	Sharp	28.5°	6.40	29.4	2.8
6	CF + Kevlar	Sharp	28.5°	4.70	29.4	2.0

Table 3. *Cont.*

Sample Number	Panel Materials	Projectile Type	Angle of Impact	Projectile Weight (g)	Impact Velocity (m/s)	Energy (J)
6	CF + Kevlar	Sharp	28.5°	5.62	57.1	7.7
7	CF + Kevlar	Smooth	28.5°	4.80	37.7	3.4
8	CF + Kevlar	Smooth	28.5°	6.09	58.8	8.9
9	CF + Kevlar	Smooth	90°	4.20	24.2	1.2
10	CF + Kevlar	Smooth	90°	4.70	76.9	13.9
11	CF + Kevlar	Sharp	90°	5.60	18.3	0.9
11	CF + Kevlar	Sharp	90°	5.60	44.4	5.5
12	CF + Kevlar	Sharp	90°	4.70	74.0	12.9
13	CF	Sharp	90°	3.10	37.7	2.2
14	CF	Sharp	90°	4.10	71.0	10.3
14	CF	Sharp	90°	6.60	45.8	6.9
14(p)	CF	Sharp	90°	6.60	102.5	34.7
15	CF	Smooth	90°	2.90	37.4	2.0
16	CF	Smooth	90°	5.70	15	0.6
16	CF	Smooth	90°	5.70	25	1.8
16 (p)	CF	Smooth	90°	5.70	74	15.6
17	CF	Sharp	28.5°	5.18	27.4	1.9
17	CF	Sharp	28.5°	4.87	33.9	2.8
18	CF	Smooth	28.5°	5.12	58.8	7.3

2.2. Samples' Analysis

An optical microscope was used to observe and analyse the damage topographies on the top and bottom surfaces of the specimens. In order to quantify the extent of the damage accurately, the thermography technique was used to measure the damaged areas. However, this non-destructive inspection method could not distinguish the damage modes. Since the focus of the work was on the surface damage, the samples were also observed to identify the key features of their surface damage.

Pulsed thermography is a reliable non-destructive testing technique for detecting near- and sub-surface damage. It is a more robust and faster method compared to ultrasonic testing and X-radiography [26]. The typical thermographic setup is illustrated in Figure 4. A pulse was emitted by a flash lamp onto the specimen's surface. Heat conduction took place on the sample and led to a decrease from the surface to the interior. An infrared (IR) camera measured the temperature of the sample surface against time. Point 1 in Figure 4 represents an undamaged area of the sample, while Point 2 represents a damaged one. In the presence of a defect, a temperature deviation occurred, and the time when it occurred (t1 in Figure 4) allowed the estimation of the defect's depth. Initially, thermographic analysis was based on contrasts in the post-heating images. Most modern systems analyse each pixel individually and independently. This allows to not be dependent of a reference standard. Thermographic signal reconstruction (TSR) allows noise reduction, and its first and second derivatives are invariant to ambient conditions, surface preparation, and input energy, thus allowing the analysis of the sub-surface of a specimen. TSR is, then, a polynomial fitting, and its first and second derivatives allow the visualisation of heat flow and heat flow variation. In this study, the model order was chosen as 7. Considering the thickness of the samples and the low thermal diffusivity of the composites, a sampling rate of 20 Hz was used, and a total of 1000 frames (equivalent to 50 s) were captured after the flash.

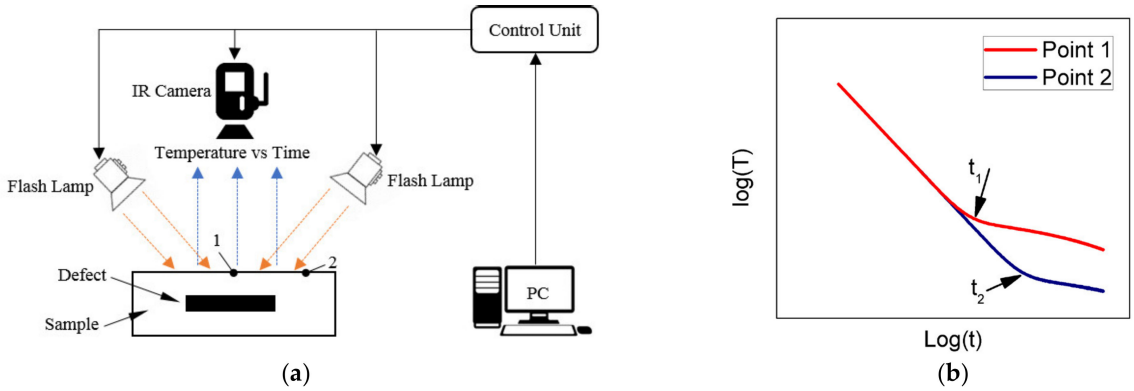

Figure 4. (**a**) Experimental configuration of the pulsed thermographic inspection under the reflection mode, where Point 1 denotes a surface location with a defect underneath and Point 2 denotes a location on the sample surface with no defect underneath. (**b**) Typical observed time–temperature decay curves in the logarithmic domain for Points 1 and 2, respectively, where the times of t1 and t2 are the key for measuring the thickness of the local materials.

3. Results and Discussion

The samples were tested with different energy levels, as described in Table 4. The results are reported by grouping together the orthogonal impact and inclined impact. The images from the optical microscopy and thermography were combined to reconstruct the internal and surface damages.

Table 4. Summary of damage observed on the composite panels under orthogonal impacts.

Sample	Material	Projectile	Energy (J)	Front Face Damage	Back Face Damage
13	CF	Sharp	2.2	Matrix cracking	No visual damage
15	CF	Smooth	2.7	Matrix cracking and indentation	Matrix crack
9	CF + Kevlar	Smooth	0.9	None	No visual damage
11	CF + Kevlar	Sharp	1.2 & 6.5	Fibre peel-off on the first layer and indentation	Matrix crack
10	CF + Kevlar	Smooth	16.9	Matrix cracking, fibre peel-off, and indentation	Cross fracture and delamination
12	CF + Kevlar	Sharp	15.6	Matrix cracking, fibre pee-off, and indentation	Cross fracture and delamination

3.1. Orthogonal Impact

A summary of the damage observed on the panels that were impacted at a 90° angle is presented in Table 4. The samples were analysed according to the following parameters: effect of the projectile surface (sharp or smooth) and the presence of a Kevlar reinforcement layer.

3.1.1. Effect of the Shape of the Projectile

CF panels 13 and 15 were impacted at 2.2 J with sharp gravel and 2.0 J with smooth gravel, respectively. Visible surface damage was observed with optical microscopy, with matrix cracking developing perpendicularly to the fibre direction in both cases. However, an indentation with a round-shaped crater was observed on panel 15, which was impacted by smooth gravel, whilst on panel 13 (sharp projectile), the matrix cracking area was larger than that on panel 15. These damages can be observed in Figures 5 and 6.

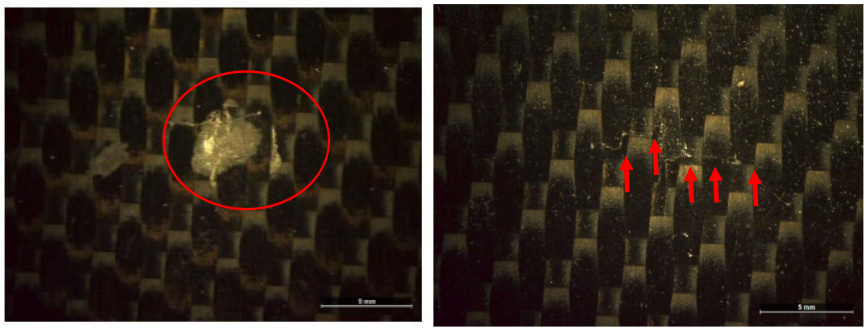

Figure 5. Optical images of the damages observed on the front faces of panels 13 (**left-hand side**) and 15 (**right-hand side**).

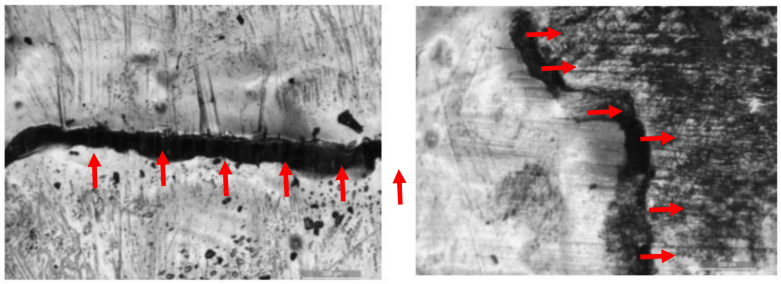

Figure 6. Optical images of the front faces of panels 13 (**left-hand side**) and 15 (**right-hand side**) detailing the matrix cracks perpendicular to the fibre direction (crack highlighted with red arrows).

The thermographic images of panels 13 and 15 allowed the identification of internal damages (Figure 7). Both panels presented similar internal damages, with indentations that were clearly identified on the front faces of the panels. On the back faces of these panels, a matrix crack in a line was noticeable on panel 13, while a different shape was observable on panel 15 (Figure 8).

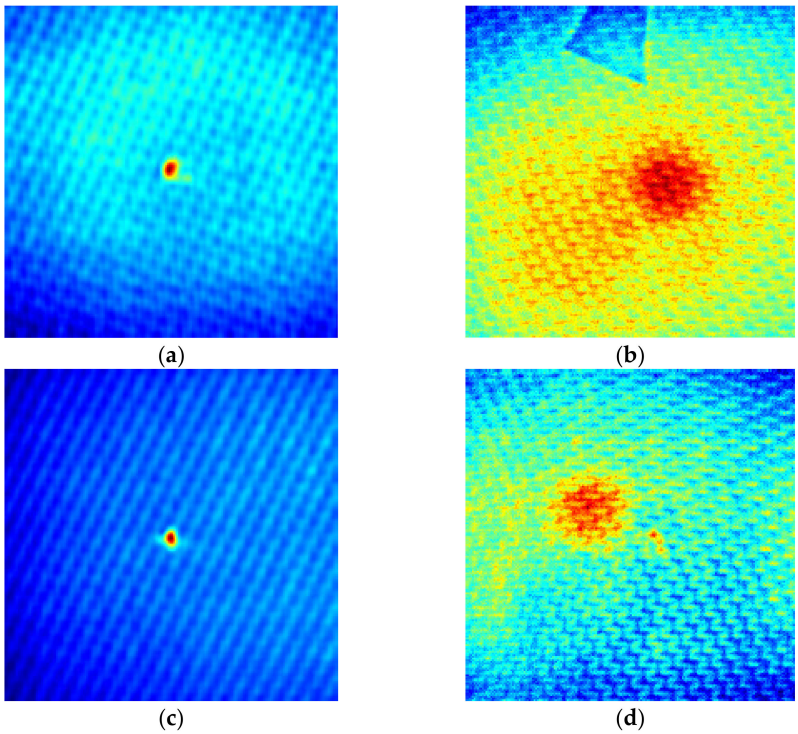

Figure 7. Thermographic images of the impact on the (**a**) front face and (**b**) back face of panel 13 and the (**c**) front face and (**d**) back face of panel 15.

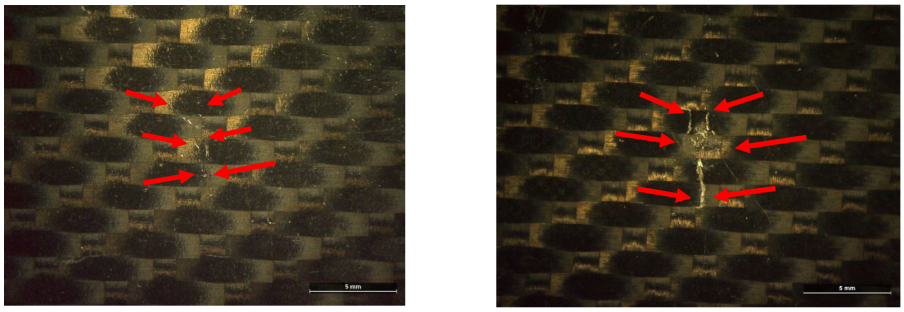

(**a**) (**b**)

Figure 8. Microscopic images of the back faces of (**a**) panel 13 and (**b**) panel 15.

3.1.2. Effect of the Layer of Kevlar for Reinforcement

Concerning the Kevlar-reinforced panels, panel 9 was impacted at 1.2 J with smooth gravel with no visible damage. In the case of panel 11, a first impact was carried out at 0.9 J with a sharp projectile. This impact created a small damaged area (the red square in Figure 9) without matrix cracking., but with fibre peel-off and failure on the first layer (Figure 10). The other marks were caused by another impact at 6.5 J with a sharp impactor (the blue triangle in Figure 9). This created a larger damaged area than the previous impact, and it was likely caused by the rotation of the gravel. The point of impact was clearly noticeable in the thermographic images (Figure 11). However, internal damages did not seem to occur (Figure 11).

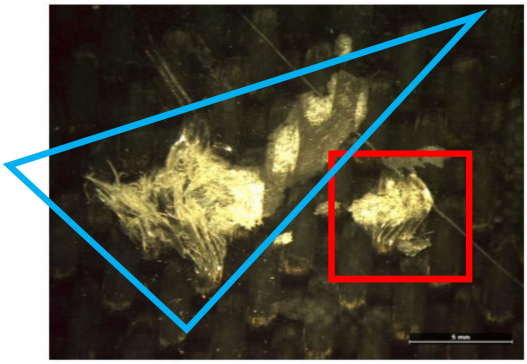

Figure 9. Optical image of the top face of panel 11 highlighting the damages cause by the first impact (red square) and the second impact (blue triangle).

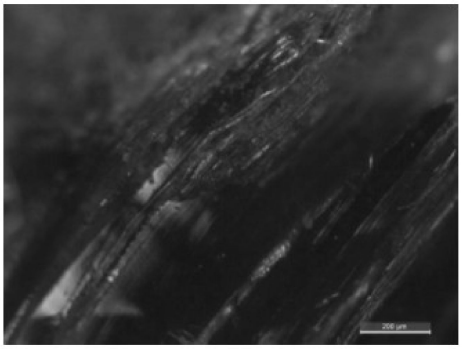

Figure 10. Microscopic image of panel 11 showing fibre loss on the first layer of the panel.

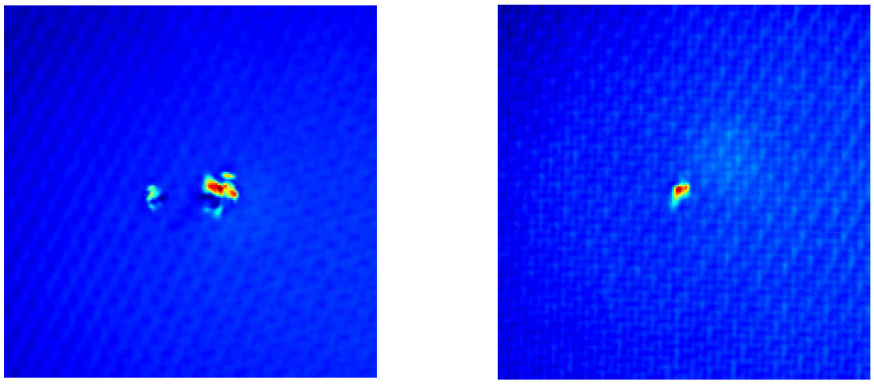

(**a**) (**b**)

Figure 11. Thermographic images of the (**a**) front face and (**b**) back face of panel 11.

On the back face, the main damage that was identifiable with optical microscopy was a matrix crack (Figure 12).

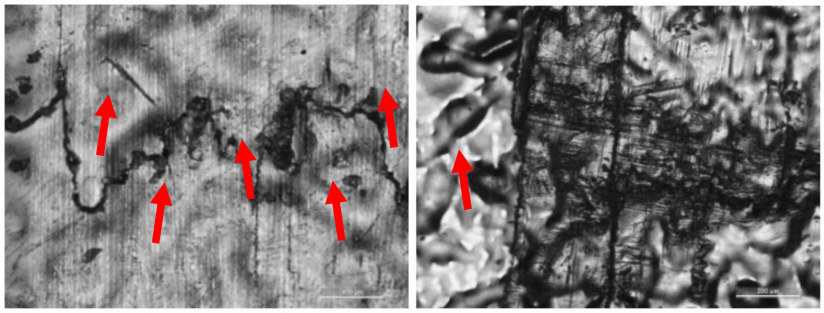

Figure 12. Microscopic images of the back face of panel 11 with a matrix crack (**left**) and localised damage (**right**).

Panels 10 and 12, which were made of CF and Kevlar, were impacted at 16.9 J with a smooth impactor and 15.6 J with a sharp one (a higher impact energy than that of panels 9 and 11), respectively. Similar damage to that of panel 11 was observed on the top face with fibre peel-off, fibre failure, and matrix damage. The thermographic and TSR images (Figures 13 and 14) illustrated a significant area of internal damages. The second derivative clearly enabled the identification of an intense but more restricted damage area close to the point of impact, which was likely delamination.

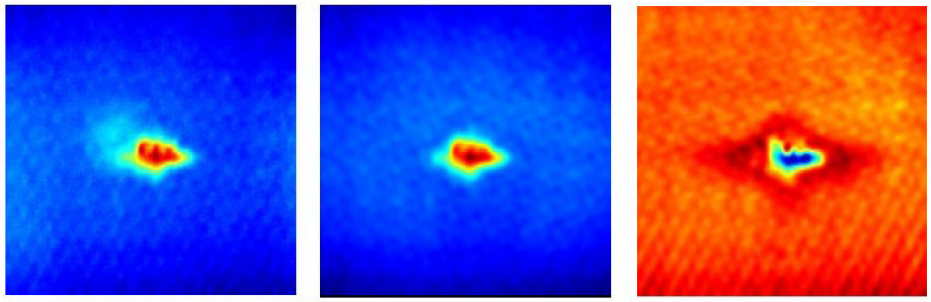

Figure 13. Thermographic images of the front face of panel 10: thermographic image (**left-hand side**), TSR image (**centre**), and second derivative (**right-hand side**).

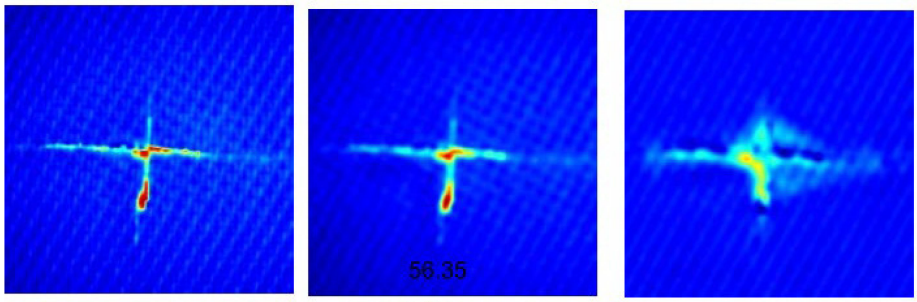

Figure 14. Thermographic images of the back face of panel 10: thermographic image (**left-hand side**), TSR image (**centre**), and second derivative (**right-hand side**).

Cross failures were observable on the back faces of the panels. The cross shape was clearly noticeable in the TSR and raw images (Figure 15). Damaged areas close to the cross were observable on the second derivative image, and they also seemed to indicate delamination.

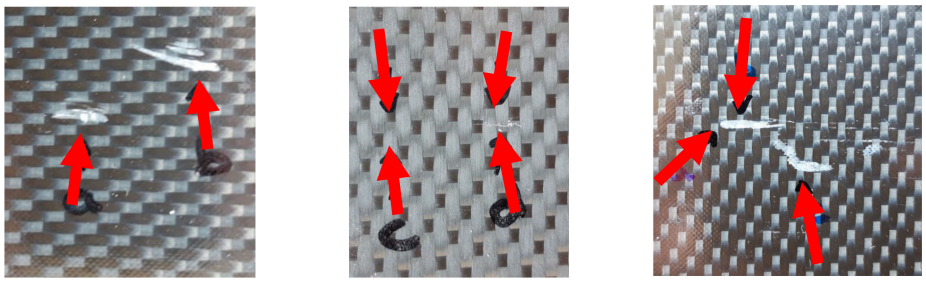

(**a**) (**b**) (**c**)

Figure 15. Images of damages on the (**a**) front face and (**b**) back face of panel 1 and on the (**c**) front face of panel 3.

3.2. Inclined Impact

A summary of the damage observed on the panels impacted at an angle of 28.5° with respect to the plane of the panel is presented in Table 5, followed by an analytical discussion on the effect of the shape of the projectile and the presence of a layer of Kevlar as reinforcement.

Table 5. Summary of the damages observed on composite panels under an inclined (28.5°) impact.

Sample	Material	Projectile	Energy	Type of Front Face Damage	Type of Back Face Damage
1	CF	Sharp	3.1 J	Matrix cracking & Fibres exposed	Matrix cracking
3	CF	Smooth	2.7 J	Fibres exposed	No visual damage
7	CF + Kevlar	Smooth	3.4 J	Scratch	No visual damage
6	CF + Kevlar	Sharp	7.7 J & 2 J	Matrix cracking & Fibre breakage	no visual damage
8	CF + Kevlar	Smooth	8.9 J	Concentration region	Matrix cracking
18	CF	Smooth	7.3 J	Matrix concentration & cracking (a,b)	Matrix cracking

3.2.1. Effect of the Shape of the Projectile

Panels 1 and 3 were impacted at 3.1 J with sharp gravel and 2.7 J with a smooth projectile, respectively, at an angle of 28.5°. Panel 1 presented damages on the front and back faces—matrix cracking and fibre peel-off—while panel 3 presented some damage only on the front face with fibre peel-off (Figure 15). The thermography images of panels 1 and 3 (Figure 16) highlighted the areas that were damaged on the front and back of the panels. The main difference between these samples and the ones that were impacted orthogonally (panels 13 and 15 in Figure 8) is the fact that, with the orthogonal impact, the damage was concentrated/localised at the contact point, while with the inclined impact, the internal damaged area is larger.

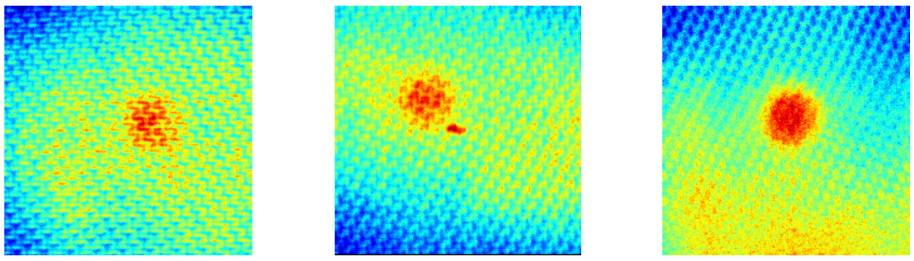

(**a**) (**b**) (**c**)

Figure 16. Thermographic images of the (**a**) front face and (**b**) back face of panel 1 and (**c**) the front face of panel 3.

3.2.2. Effect of the Layer of Kevlar for Reinforcement

To assess the effect of the Kevlar layer with an inclined impact, panels 3 and 7 were compared. These panels were impacted with smooth projectiles at 2.7 and 3.4 J, respectively; panel 7 was the one with the layer of Kevlar for reinforcement. On panel 7, the front face presented some scratches, while the back face had no visible damage (Figure 17). The levels of damage obtained were similar for both panels, suggesting that the reinforcement layer of Kevlar had little effect.

(**a**) (**b**) (**c**)

Figure 17. Images of the front face of panel 7: (**a**) microscopic image showing damage from the impact, (**b**) magnification showing matrix cracking, and (**c**) thermographic image showing internal damages.

Panels 6 and 18 were impacted at 7.7 J with a sharp projectile and 7.3 J with a smooth projectile, respectively, with both at an angle of 28.5°. Both panels presented scratches in the area of the impact. However, panel 6 did not present damage on its back face, while panel 18 had a matrix crack (Figure 18).

In this case, the smooth projectile caused more layer damage to the panel than the sharp one did. This could be related to the effect of the reinforcement of the Kevlar layer in the panel configuration. At low levels of impact energy, the effect of the Kevlar layer was not observed, but at higher levels, it reduced the damage on the back face of the plate. However, some internal damage was identified (Figure 19).

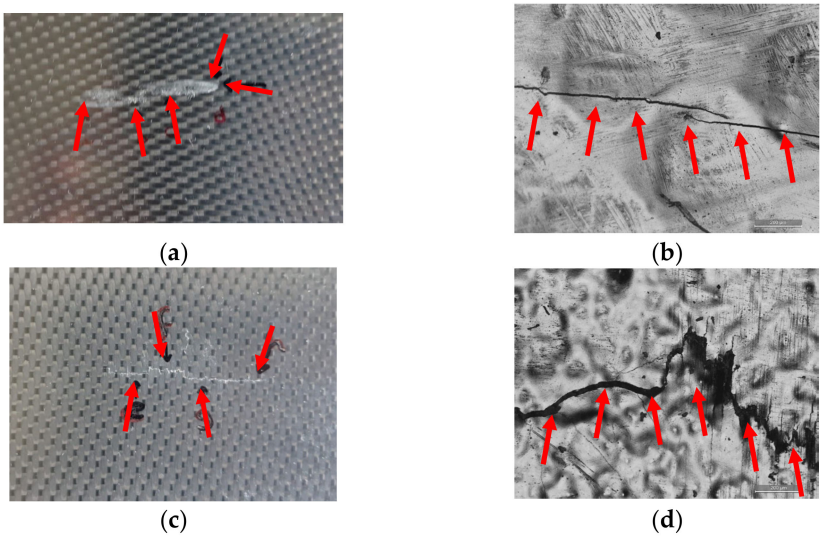

Figure 18. Microscopic images of panel 18: (**a**) front face, (**b**) magnification of the front face, (**c**) back face, and (**d**) magnification of the back face.

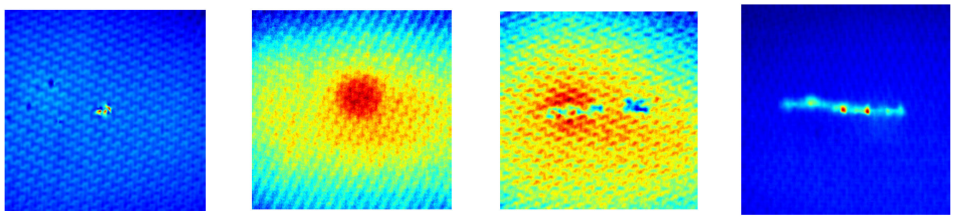

Figure 19. Thermographic images of the (**a**) front face and (**b**) back face of panel 6 and the (**c**) front face and (**d**) back face of panel 18.

In terms of the angle of impact, by comparing panels 3 and 15, it was noticed that inclined impacts caused less damage on the composite panels than perpendicular impacts did.

3.3. Effect of Impact Energy

For the plate thicknesses of 1.05 and 1.40 mm, several levels of damage were observed in relation to the impact energy. For a low level of energy (2–6 J), damage on the top surface was observed; for a medium level (6–14 J), there was visible damage on the front and back faces and through the thickness; for high levels (higher than 15 J), total penetration of the plates occurred. However, the effect of the reinforcement with the Kevlar layer was evident. For example, when impacted with a smooth projectile, plate 4 (CF lay-up) suffered penetration at an impact energy of 11.6 J, while plate 10 (CF + Kevlar lay-up) did not experience penetration at an impact energy of 13.9 J.

Further investigation of the impact through the images captured with a high-speed camera showed a contribution of the Kevlar layer to a reduction in the amount of damage produced on the front face. Figures 20–23 show sequences of three frames captured during the test to show the start of the impact, an intermediate position, and the final position of the gravel before it detached from the specimen. The four different sequences refer to orthogonal and inclined impacts with either sharp or smooth gravel. The gravel, which was either sharp or round, produced limited damages on the surfaces when the panels were reinforced with a Kevlar layer on the bottom face. The sharp gravel could cut the panel, with partial perforation and extensive damages, whilst the round gravel impacted the surface and rolled over it, as happened without the Kevlar reinforcement, producing a fibre cut and scratches in the resin. These impact conditions refer to energy levels that did not produce perforation.

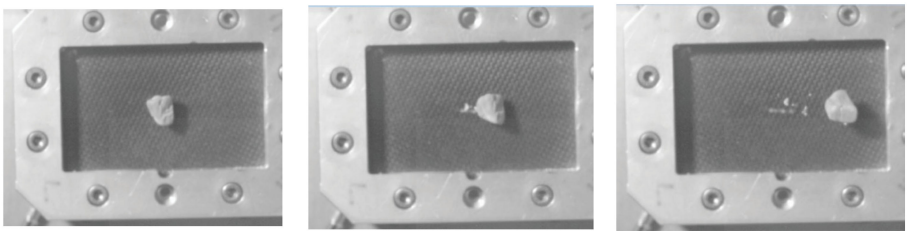

Figure 20. Sample 5, sharp gravel, CF + Kevlar, 2.8 J, showing the initial (**left**), intermediate (**centre**), and gravel detachment stages (**right**).

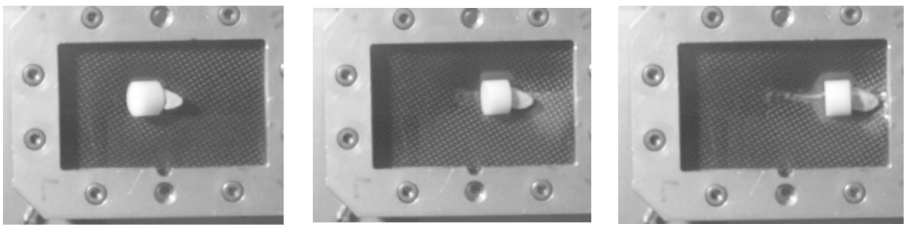

Figure 21. Sample 2 (CF, 28.5 degrees, 15.4 J), test n. 19, sharp gravel, showing the initial (**left**), intermediate (**centre**), and gravel detachment stages (**right**).

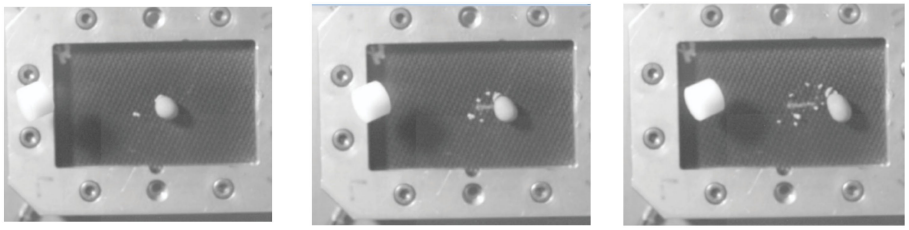

Figure 22. Sample 7, CF + Kevlar, 3.4 J, smooth gravel, showing the initial (**left**), intermediate (**centre**), and gravel detachment stages (**right**).

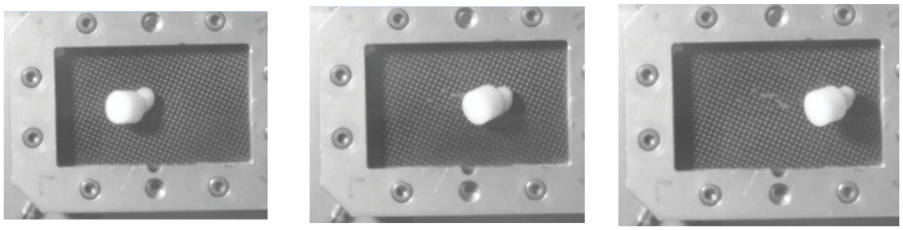

Figure 23. Sample 3, CF, smooth gravel, 2.7 J, 28.5 degrees, showing the initial (**left**), intermediate (**centre**), and gravel detachment stages (**right**).

If we compare our observations with the previous literature review, the same damages as those observed by Liu et al. [24] were noticed for panels 10, 12, and 14. The damages were caused by compressive stress waves generated and transmitted through the volume after impact. These waves were then reflected on the back face of the panel and formed tensile waves, thus explaining the fibre failure on the back face. It is then likely that delamination occurred. Compared with the results from Othman et al. [27], who assessed impacts on unidirectional laminates, the damages were different. The matrix cracks were in the direction of the fibres, while with these woven panels, the cracks were perpendicular to the fibres.

4. Conclusions

Gas gun testing for high-velocity impacts was used to characterize the responses of composite panels that were impacted under different energy levels and different angles by gravel of different shapes.

Sharp gravel produced more damage on the top face compared to smooth gravel, whilst the damage on the back face was not affected by the shape, but only by energy and angle. From the thermographic results, more internal damages were observed with sharp gravel, but this would need to be confirmed through further analyses.

Matrix damage was the main mechanism observed at a low impact energy (around 2 J), whilst at higher energies, Kevlar delayed the fibre damages by improving the ballistic limits of the panels. However, at a low level of energy, no major improvements were noticed when using Kevlar, as matrix cracking was dominant.

Further work on the through-thickness analysis of the panels is required, as thermography cannot provide a definitive answer.

Author Contributions: Data curation, V.M.R., M.G.; Formal analysis, V.M.R., M.G.; Experimental Data A.R., M.G., V.M.R., K.D., H.L.; Writing—original draft, M.G., V.M.R.; Review & Editing, M.G., V.M.R., Y.Z., A.R., G.J.A.-T. All authors have read and agreed to the published version of the manuscript.

Funding: This research received no external funding.

Institutional Review Board Statement: Not applicable.

Informed Consent Statement: Not applicable.

Data Availability Statement: The data that support the findings of this study are available on request from the corresponding author. The data are not publicly available due to privacy or ethical restrictions.

Acknowledgments: The Authors would like to thank Nick Smith and SHD Composites for supplying the composite materials.

Conflicts of Interest: The authors declare no conflict of interest.

References

1. Ursenbach, D.O. Penetration of CFRP Laminates by Cylindrical Indenters. Master's Thesis, The University of British Columbia, Vancouver, BC, Canada, October 1995.
2. Bhatnagar, A. *Lightweight Ballistic Composites*; Woodhead Publishing: Sawston, UK, 2006. [CrossRef]
3. Cantwell, W.J.; Morton, J. Comparison of the low and high velocity impact response of CFRP. *Composites* **1989**, *20*, 545–551. [CrossRef]
4. Vaidya, U.K. Impact response of laminated and sandwich composites. In *Impact Engineering of Composite Structures*; Abrate, S., Ed.; Springer: Vienna, Austria, 2011; pp. 97–191. [CrossRef]
5. Mitrevski, T.; Marshall, I.H.; Thomson, R. The influence of impactor shape on the damage to composite laminates. *Compos. Struct.* **2006**, *76*, 116–122. [CrossRef]
6. Cantwell, W.J.; Morton, J. Impact perforation of carbon fibre reinforced plastic. *Compos. Sci. Technol.* **1990**, *38*, 119–141. [CrossRef]
7. Shahkarami, A.; Cepus, E.; Vaziri, R.; Poursartip, A. Material responses to ballistic impact. *Lightweight Ballist. Compos. Mil. Law-Enforc. Appl.* **1995**, *2*, 72–100. [CrossRef]
8. Andrew, J.J.; Srinivasan, S.M.; Arockiarajan, A.; Dhakal, H.N. Parameters influencing the impact response of fiber-reinforced polymer matrix composite materials: A critical review. *Compos. Struct.* **2019**, *224*, 111007. [CrossRef]
9. Børvik, T.; Langseth, M.; Hopperstad, O.S.; Malo, K.A. Perforation of 12 mm thick steel plates by 20 mm diameter projectiles with flat, hemispherical and conical noses: Part I: Experimental study. *Int. J. Impact Eng.* **2002**, *27*, 19–35. [CrossRef]
10. Hoskin, B.C.; Baker, A.A. *Lectures on Composite Materials for Aircraft Structures*; Aeronautical Research Labs: Melbourne, Australia, 1982.
11. Tang, E.; Wang, J.; Han, Y.; Chen, C. Microscopic damage modes and physical mechanisms of CFRP laminates impacted by ice projectile at high velocity. *J. Mater. Res. Technol.* **2019**, *8*, 5671–5686. [CrossRef]
12. Beland, S. *High Performance Thermoplastic Resins and Their Composites*, 1st ed.; William Andrew: Norwich, NY, USA, 1990.
13. Vieille, B.; Casado, V.M.; Bouvet, C. About the impact behavior of woven-ply carbon fiber-reinforced thermoplastic-and thermosetting-composites: A comparative study. *Compos. Struct.* **2013**, *101*, 9–21. [CrossRef]
14. Lopes, C.; Seresta, O.; Abdalla, M.; Gurdal, Z.; Thuis, B.; Camanho, P. Stacking sequence dispersion and tow-placement for improved damage tolerance. In Proceedings of the 49th AIAA/ASME/ASCE/AHS/ASC Structures, Structural Dynamics, and Materials Conference, 16th AIAA/ASME/AHS Adaptive Structures Conference, 10th AIAA Non-Deterministic Approaches Conference, 9th AIAA Gossamer Spacecraft Forum, 4th AIAA Multidisciplinary Des., Schaumburg, IL, USA, 7–10 April 2008; p. 1735.

15. York, C.B. Unified approach to the characterization of coupled composite laminates: Benchmark configurations and special cases. *J. Aerosp. Eng.* **2010**, *23*, 219–242. [CrossRef]
16. Dorey, G. Failure Mode of Composite Materials with Organic Matrices and Their Consequences in Design. 1975. Available online: https://apps.dtic.mil/sti/citations/ADA018178 (accessed on 31 July 2022).
17. Park, R.; Jang, J. Impact behavior of aramid fiber/glass fiber hybrid composites: The effect of stacking sequence. *Polym. Compos.* **2001**, *22*, 80–89. [CrossRef]
18. Abrate, S. *Impact Engineering of Composite Structures*; Springer Science & Business Media: Berlin/Heidelberg, Germany, 2011; Volume 526.
19. Gellert, E.P.; Cimpoeru, S.J.; Woodward, R.L. A study of the effect of target thickness on the ballistic perforation of glass-fibre-reinforced plastic composites. *Int. J. Impact Eng.* **2000**, *24*, 445–456. [CrossRef]
20. Icten, B.M.; Kıral, B.G.; Deniz, M.E. Impactor diameter effect on low velocity impact response of woven glass epoxy composite plates. *Compos. Part. B Eng.* **2013**, *50*, 325–332. [CrossRef]
21. Sevkat, E.; Liaw, B.; Delale, F. Drop-weight impact response of hybrid composites impacted by impactor of various geometries. *Mater. Des. 1980–2015* **2013**, *52*, 67–77. [CrossRef]
22. Safri, S.N.A.; Sultan, M.T.H.; Yidris, N.; Mustapha, F. Low velocity and high velocity impact test on composite materials—A review. *Int. J. Eng. Sci* **2014**, *3*, 50–60.
23. Lee, S.-M.; Cheon, J.-S.; Im, Y.-T. Experimental and numerical study of the impact behavior of SMC plates. *Compos. Struct.* **1999**, *47*, 551–561. [CrossRef]
24. Liu, J.; Liu, H.; Kaboglu, C.; Kong, X.; Ding, Y.; Chai, H.; Blackman, B.R.; Kinloch, A.J.; Dear, J.P. The impact performance of woven-fabric thermoplastic and thermoset composites subjected to high-velocity soft- and hard-impact loading. *Appl. Compos. Mater.* **2019**, *26*, 1389–1410. [CrossRef]
25. Gustin, J.; Joneson, A.; Mahinfalah, M.; Stone, J. Low velocity impact of combination Kevlar/carbon fiber sandwich composites. *Compos. Struct.* **2005**, *69*, 396–406. [CrossRef]
26. Zhao, Y.; Addepalli, S.; Sirikham, A.; Roy, R. A confidence map based damage assessment approach using pulsed thermographic inspection. *NDT E Int.* **2018**, *93*, 86–97. [CrossRef]
27. Othman, R.; Ogi, K.; Yashiro, S. Characterization of microscopic damage due to low-velocity and high-velocity impact in CFRP with toughened interlayers. *Mech. Eng. J.* **2016**, *3*, 16-00151. [CrossRef]